Design of a Single-Hit Neutron Spectrometer for D-D Fusion

Henry Berger

Brighton High School

LLE Advisor: Chad Forrest

February 2020

Laboratory for Laser Energetics

University of Rochester

1 Abstract

A neutron spectrometer was designed and simulated for use with 2.45 MeV neutrons from fusion reactions with durations beyond the limits of current modes of time-of-flight-based spectroscopy. This diagnostic will be used to infer the apparent temperature of fusing ions. The spectrometer consists of two parts: a deuterated plastic converter foil, in which an incident neutron can transfer its energy to a deuteron, and a silicon complementary metal-oxide-semiconductor (CMOS) chip that measures the energy of deuterons. The shape of the observed deuteron energy spectrum was found to be strongly predictive of the shape of the incident neutron energy spectrum, enabling the determination of the fusing particles' apparent thermal energy. Many design parameters, including the converter's material, thickness, and distance from the detector, were optimized in order to maximize the detection rate and energy resolution. Simulations were used to determine the range of neutron yields and ion temperatures for which the spectrometer would be effective. The neutron yield at FuZE, the reactor for which the spectrometer was designed, is too low for the spectrometer to function, but other existing fusion reactors, such as JET, have sufficient neutron yields. A spectrometer based on this work will be built at LLE.

2 Introduction

2.1 Nuclear fusion

Nuclear fusion is the process by which two nuclei combine to form a single nucleus. All nuclei have positive charge, so fusion requires overcoming the Coulombic repulsion between the two nuclei. Once the two nuclei move close enough together, a nuclear force dominates, causing the nuclei to fuse. This effect is shown in Figure 1.

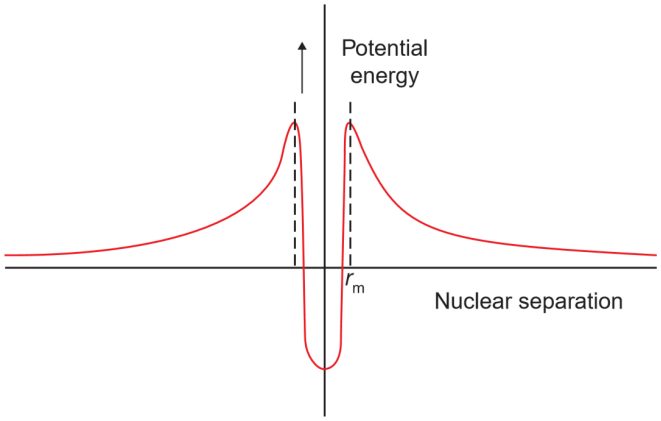

Figure 1: *Potential energy vs. separation for two positively charged nuclei. Above r_m, the Coulombic force is dominant, causing the two nuclei to repel. At distances less than r_m, the nuclear attraction exceeds the Coulombic repulsion, causing the two nuclei to fuse.*[1]

Most fusion research uses deuterium (hydrogen with one neutron, abbreviated D), often in combination with tritium (hydrogen with two neutrons, abbreviated T) or helium-3 (helium with only one neutron, abbreviated ^{3}He). Reactions with these isotopes are preferred because they have relatively high cross-sections, or likelihoods of occurrence. The three most likely candidates for fusion reactions are:

- D-D Fusion: $D + D \rightarrow {}^3He + n$ (2.45 MeV)
- D-T Fusion: $D + T \rightarrow {}^4He + n$ (14.1 MeV)
- D-^{3}He Fusion: $D + {}^3He \rightarrow {}^4He + p^+$ (14.7 MeV),

where n represents a neutron and p^+ represents a proton.[1]

The cross-section of a reaction depends on the energy of the fusing particles. If the ions have too little energy, they cannot overcome the Coulombic repulsion. If the ions have too much energy, they move so quickly that they are less likely to fuse. The dependence of cross-section on ion energy is shown in Figure 2.

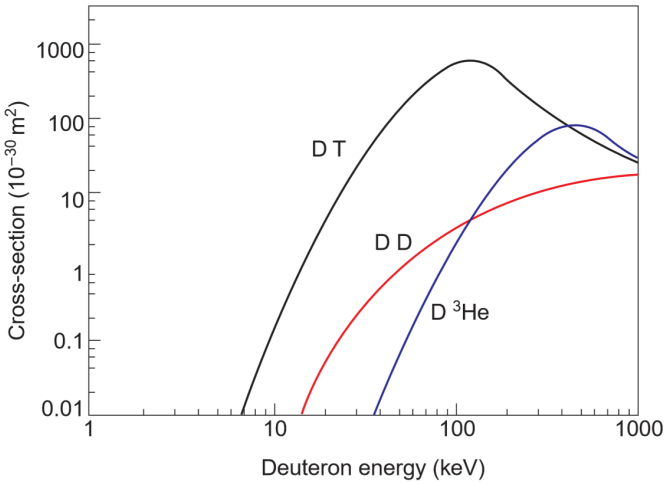

Figure 2: *Cross-sections of common fusion pathways vs. deuteron energy. The cross-section measures the probability of a fusion reaction occurring. Specifically, if the fusing ions were solid spheres that fuse whenever they touch, the cross-section would be their geometrical cross-section. Larger cross-sections indicated a greater probability of fusion.*[1]

2.2 Nuclear fusion reactors

Controlled nuclear fusion requires confining a plasma to a limited volume for enough time for fusion to occur. Nuclear fusion reactors are classified as either inertial confinement fusion (ICF) or magnetic confinement fusion (MCF), depending on the method of confining the plasma.

In ICF, a small capsule of fuel is compressed by a short, intense burst of radiation. The ablation of the outside of the capsule forces the contents inward, and fusion occurs at extremely high pressure and density. The fusion ends when the power released by the fusion causes the fuel to expand to a greater volume and lower density. Because only the fuel's inertia slows the expansion of the fuel, the duration of fusion is very

short, on the order of nanoseconds. Most ICF facilities, such as the National Ignition Facility (NIF) and the OMEGA facility, use laser pulses to compress the capsules.[1]

MCF uses magnetic fields to confine the fusing plasma. Current is passed through a plasma, generating a magnetic field that compresses the plasma. The magnetic field produced by the plasma is often enhanced by external magnets. Because a magnetic field confines the plasma, MCF reactors can maintain the temperature and density required for fusion for longer durations than ICF reactors can achieve. Many MCF reactors, such as the Joint European Torus (JET), use a toroidal design called a tokamak.[1] The spectrometer described in this work is intended for use at the Fusion Z-Pinch Experiment (FuZE), an experimental fusion reactor located at the University of Washington, Seattle. The reactor at FuZE is a variant of MCF called a Z-pinch reactor, in which the shape of the fusing plasma is linear, not toroidal.[2]

2.3 Neutron spectroscopy

Ion temperature directly affects the likelihood of fusion, so ion temperature is one of the most important diagnostics for evaluating how close a reactor is to achieving a sustained fusion reaction. A common method of determining the ion temperature of a fusing plasma is to analyze the neutron spectrum produced by the plasma. The temperature determined from the neutron spectrum is averaged over the entire time and volume of fusion, and it is also affected by which neutrons are able to escape the reactor. For this reason, this temperature is called the apparent, or neutron-averaged, temperature, as opposed to the true thermal temperature. The true thermal temperature of the fusing plasma varies with time and space and is more difficult to measure, so most diagnostics instead measure the apparent temperature.

The neutron spectrum produced by a plasma with ion temperature T_i is given by

$$f(E_n)dE_n = dE_n \exp\left[-\frac{(E_n - \langle E_n \rangle)^2}{\left(\frac{4m_n T_i \langle E_n \rangle}{m_n + m_\alpha}\right)}\right], \tag{1}$$

where E_n is neutron energy; $f(E_n)dE_n$ is the relative probability density of the neutron spectrum at E_n; $\langle E_n \rangle$ is the mean energy, which varies slightly based on T_i; m_n is the mass of a neutron; and m_α is the mass of the other particle produced by the reaction, which is a ^3He nucleus in the case of D-D fusion.[3] This is a Gaussian function, of the form

$$f(x)dx = \frac{dx}{\sigma\sqrt{2\pi}} \exp\left[-\frac{(x - \bar{x})^2}{2\sigma^2}\right].$$

It follows that the standard deviation, σ, is related to the temperature by

$$2\sigma^2 = \frac{4m_n T_i \langle E_n \rangle}{m_n + m_\alpha}, \tag{2}$$

and thus

$$T_i = \frac{\sigma^2 \left(m_n + m_\alpha\right)}{2 m_n \langle E_n \rangle}. \tag{3}$$

As a result, the apparent temperature can be inferred from knowledge of the σ and $\langle E_n \rangle$ of the neutron spectrum. Two of the most common methods of measuring the neutron spectrum are time-of-flight spectroscopy and charged particle spectrometry.[4]

Time-of-flight spectroscopy determines neutron energy by measuring the time taken for a neutron to travel a known distance. Dividing the distance by the time yields the neutron's velocity, which can be used to determine its energy. Time-of-flight measurement relies upon precise knowledge of the time and location at which neutrons are generated. As a result, time-of-flight spectroscopy is often used with fusion reactors that have very small targets that fuse over very short intervals. ICF reactors primarily use time-of-flight neutron spectroscopy.

Charged particle spectrometry, by contrast, detects neutron energy more indirectly. Neutrons hit a converter foil, where they produce charged particles in recoil reactions. The energy of the charged particle can be used to determine the energy of the incident neutron. The method of measuring the energy of the charged particle varies. The Magnetic Recoil Spectrometer (MRS), at the NIF and OMEGA facilities, uses a powerful magnet that bends the paths of protons and deuterons by angles dependent on their velocities. For high accuracy, charged particle spectrometers require very high yields, because they have low detection rates. For example, the MRS detects less than 1 out of every 10^9 neutrons created in the fusion volume.[5]

2.4 FuZE

The ion temperature at FuZE is estimated to be $1 - 2\ keV$.[2] However, a more precise measurement is difficult, because the long duration and low neutron yield of FuZE complicate the use of existing neutron spectrometers. FuZE uses D-D fusion, so the spectrometer was designed for the 2.45 MeV neutrons produced by D-D fusion.

FuZE has a fusion duration of approximately 5 μs.[2] A conventional time-of-flight spectrometer at a distance of around 10 m must know the time of flight to within a few picoseconds in order to make an accurate estimate of temperature.[6] Therefore, microseconds of uncertainty in the time of generation of a neutron make conventional neutron time-of-flight spectrometry extremely challenging. It might be possible to use a ^3He start/stop gate to measure the time of generation of each neutron, but such a method would be very difficult. With regard to charged-particle spectrometry, the yield at FuZE is on the order of 10^5 neutrons per pulse over 4π steradians.[2] This is multiple orders of magnitudes too low for the use of spectrometers like the MRS, with detection rates on the order of 10^{-9}. The spectrometer developed in this work was designed to accomodate the long duration and low yield of FuZE.

3 Design of the spectrometer

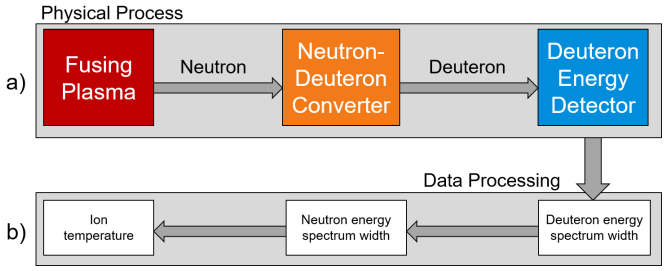

Figure 3: *Schematic of the neutron spectroscopy approach. a) The physical process. b) The post-processing of the data.*

The spectrometer investigated in this project uses a design similar to that of other charged particle spectrometers. First, incident neutrons encounter a converter foil. Neutrons collide with atoms in the foil, producing charged particles. Deuterated plastic, which produces deuterons when bombarded by neutrons, was chosen as the material for the converter foil, for reasons that will be discussed below. The deuterons then leave the foil and hit an energy detector, which registers the deuteron energy. The width of the deuteron energy distribution is then used to calculate the width of the neutron energy spectrum, which is used to calculate the apparent temperature of the fusing ions. This process is shown schematically in Figure 3 and physically in Figure 5 below.

The deuteron energy detector was chosen to be Icarus, a high-speed complementary metal-oxide-semiconductor (hCMOS) chip produced by Sandia National Laboratories, as shown in Figure 4(a). Icarus consists of a 9 μm-thick layer of silicon, which is divided into a 512×1024 array of pixels.[7] As deuterons pass through the silicon sheet, they deposit energy, which is converted into an electrical pulse. The sensor measures the height of this pulse, which can be used to determine the energy of the deuteron. The chip detects the energy of individual deuterons, hence the classification of the spectrometer as a single-hit spectrometer. Icarus has a frame duration of 1.5 ns,[7] so if two deuterons hit the same pixel of the chip within 1.5 ns, they will be counted as a single deuteron that creates a larger pulse. In the conditions examined in this work, the deuteron flux was low enough that double hits were extremely unlikely.

The Icarus chip is too thin to fully stop incident deuterons. The rate of energy loss, $\frac{-dE}{dx}$, of a particle in silicon is dependent on the particle's energy, E, by

$$\frac{-dE}{dx} = \frac{C_1}{E}\left[\ln\left(\frac{E}{C_2 - E}\right) + C_3 - \frac{E}{C_2}\right], \tag{4}$$

where C_1, C_2, and C_3 are constant with respect to E.[8] This relation is dominated by the $\frac{1}{E}$ term, so the higher the energy of the particle, the less energy it deposits. In the range of $1 - 2.5\ MeV$, deuterons deposit approximately $0.1 - 0.25\ MeV$. The relationship between deuteron energy and deposited energy is show in

Figure 4(b).

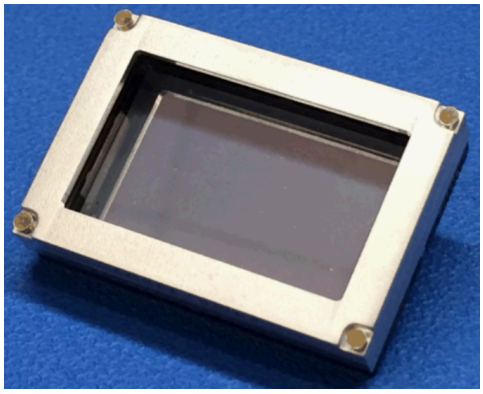

(a) The Icarus hCMOS chip, produced by Sandia National Laboratories, which was chosen as the deuteron detector.

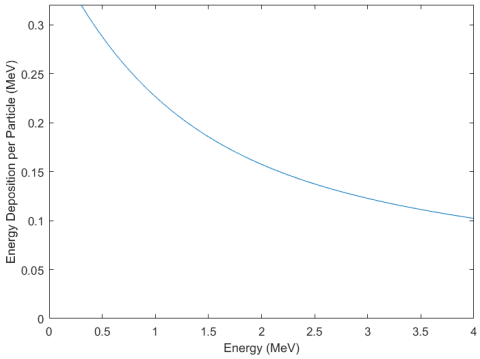

(b) Energy deposition of deuterons in the 9 μm silicon layer of Icarus, as predicted by Eq. 4. MCNP simulations confirmed these predictions. Deuterons with energies below approximately 0.3 MeV (not shown) deposit all their energy and do not escape the surface. This is called ranging out.

Figure 4: *The Icarus hCMOS chip, and the energy deposition of deuterons in the chip.*

4 Initial optimization of the spectrometer design

The optimization of the spectrometer design examined four characteristics of the spectrometer, as shown in Figure 5:

- The maximum observable scattering angle, θ_{max}. This is the maximum angle between the velocity of a deuteron hitting the detector surface and the velocity of the incident neutron that produced the deuteron. The maximum scattering angle was controlled by changing the distance between the converter foil and detector surface, labeled d in Figure 5.
- The material of the converter foil.
- The mass thickness, $\langle \rho l \rangle$, of the converter foil, which is the product of its density and thickness.
- The configuration of the detector surface relative to the converter foil. Figure 5 shows a planar configuration, which is optimal.

Due to dependencies of the different characteristics on each other, they were optimized in pairs. The converter foil material and the detector surface configuration were optimized in combination, and then the mass thickness of the converter foil and the maximum scattering angle were optimized in combination. All optimization of the spectrometer was performed using simulations using Monte Carlo N-Particle Code (MCNP).[9]

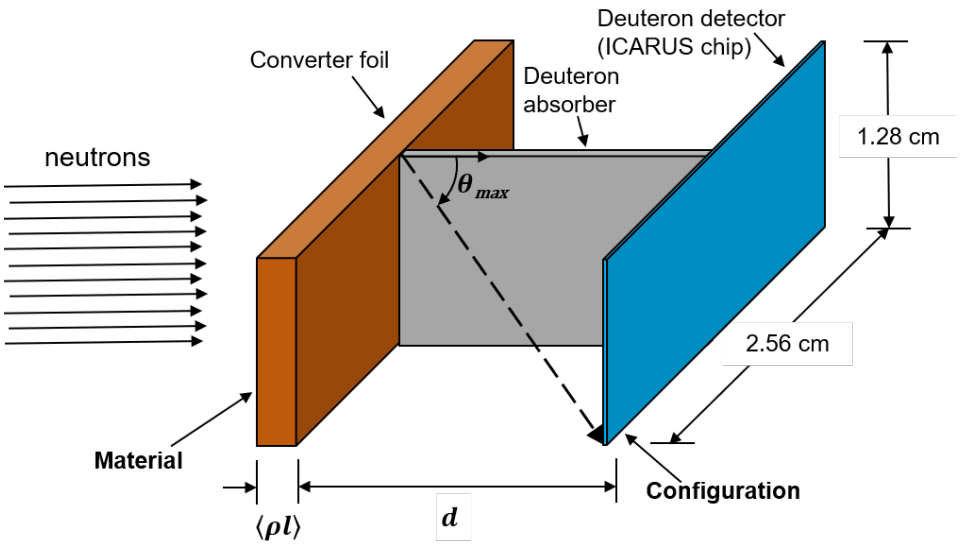

Figure 5: *Design of the spectrometer. The four parameters investigated were the maximum observable scattering angle, θ_{max}, the material of the converter foil, the mass thickness of the converter foil, $\langle \rho l \rangle$, and the configuration of the detector relative to the converter foil. The Icarus chip, shown here as a single detector, consists of 2^{19} independent pixels, each capable of detecting individual deuterons. The deuteron absorber is discussed in Section 4.3.*

4.1 Configuration of detector(s) around the converter

The spectrometer was originally designed as an array of macropixels, with each macropixel consisting of a converter foil and detector surface. The term macropixel is used to differentiate from the pixels of Icarus, which are contained within the macropixels. The detector surface could be configured in multiple different ways relative to the converter foil. The macropixels are arranged along the plane normal to the direction of neutron travel (henceforth the detection plane), so the ideal macropixel arrangement would maximize neutron detection while minimizing the area of the detection plane that is occupied. The following four arrangements were considered, as shown in Figure 6.

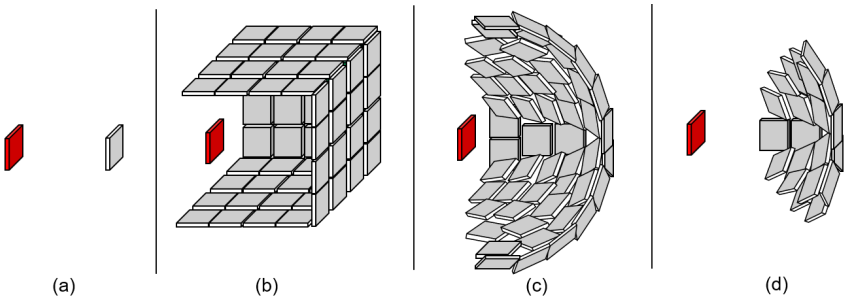

Figure 6: *The four arrangements considered. a) Planar. b) Rectangular prismic. c) Hemispherical. d) Spherical cap.*

1. **Planar.** In this arrangement, the detector surface is planar and is equal in shape and area to the converter foil.

2. **Rectangular prismic.** The converter foil and detector surface form a rectangular prism, where the converter foil is one base and the detector surface comprises the other five faces.
3. **Hemispherical.** The detector surface forms a hemisphere around the converter foil.
4. **Spherical cap.** The detector surface forms a section of a sphere, with the converter foil at its center.

All four arrangements are, in essence, variants of the spherical cap arrangement. A spherical cap with a large angle is a hemisphere; a spherical cap with a small angle approaches the planar arrangment. The rectangular prismic and hemispherical arrangements both capture 2π steradians of deuterons, so they have no relevant differences. Therefore, an examination of spherical cap arrangements with different maximum angles covered all cases.

The space-efficiency of each arrangement depends on how many particles the arrangement can detect. This depends on the angular distribution of the charged particles produced by the converter foil, which in turn depends on the material of the converter foil. For this reason, arrangements were considered in combination with materials.

4.2 Material of the converter foil

The purpose of the converter foil is to produce detectable charged particles when bombarded with neutrons. Therefore, the ideal converter foil material would produce as many charged particles as possible per incident neutron. Five materials were considered, as shown in Table 1.

Table 1: *Materials Investigated*

Converter Foil Material	**Charged Particle Produced**
Hydrogen (H_2)	Proton (p^+)
Plastic (CH_2)	Proton (p^+)
Deuterium (D_2)	Deuteron (np^+, or d^+)
Deuterated plastic (CD_2)	Deuteron (np^+, or d^+)
Helium-3 (^3He)	Helion (np_2^{2+}, or $^3He^{2+}$)

Each material has a different cross-section for charged particle-producing reactions, meaning that it produces different numbers of charged particles at each angle. To determine the ideal material and detector configuration, each material's performance was simulated with spherical cap configurations with central angles ranging from 2.5° to 90°. The simulations tracked the number of charged particles detected by the detector surface, divided by the area of the detector plane occupied by the detector surface. The simulation used a very thin converter foil, so that the charged particles would experience minimal energy loss while escaping the foil. The results are shown in Figure 7.

The simulations did not take into account any bonds between atoms. Therefore, CH_2 and CD_2 produced exactly 2/3 as many charged particles as H_2 and D_2, respectively. The plastics CH_2 and CD_2 are both solids

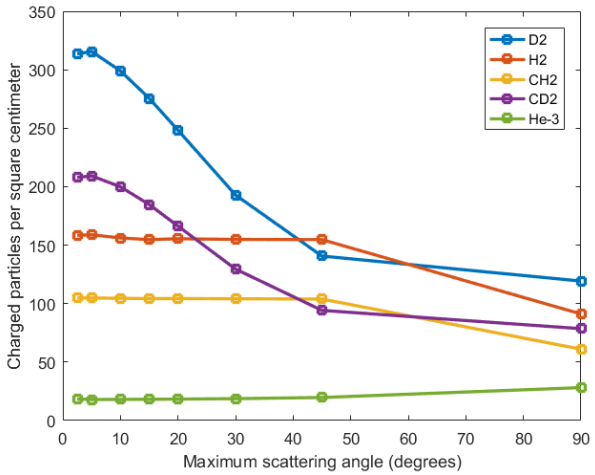

Figure 7: *Space-efficiency of spherical cap configurations for different angles and materials. The detection rate per unit area depends upon the number density of the atoms of the material, the number of incident neutrons, and the distance between the converter foil and the detector surface. These parameters were* 0.1 mol/cm^3, 10^7 *neutrons, and* 1 cm, *respectively, for all trials.*

at room temperature, whereas H_2, D_2, and ^3He are gases. Therefore, in order to reach comparable number densities, H_2, D_2, and ^3He would have to be cooled to liquids, at cryogenic temperatures. This would substantially increase the cost and difficulty of fabricating the converter foil. There is no overwhelming advantage to using H_2 or D_2, because the charged particle production rates of H_2, CH_2, D_2, and CD_2 are all within about a half order of magnitude of each other, and the production rate of ^3He is significantly lower. Therefore, further comparisons were limited to the solid materials, CH_2 and CD_2.

Between CH_2 and CD_2, CD_2 has a higher space-efficiency at angles less than 40 degrees; CH_2 is marginally better at 45 degrees, and CD_2 is better at 90 degrees. CD_2's greatest space-efficiency, which is at low angles, is twice the maximum space-efficiency of CH_2, and CD_2 is more space-efficient at most angles sampled. For this reason, CD_2 was chosen as the material for the converter foil.

The highest space-efficiency for CD_2 occurs at low angles. At low angles, the spherical cap configuration is very similar to a planar Icarus, so a planar configuration was chosen. The planar shape of the Icarus chip also facilitates the choice of a planar configuration.

The Icarus chip has dimensions 1.28 $cm \times 2.56$ cm, with a thickness of 9 μm.[7] The sensor is divided by a deuteron absorber into two square panels, or macropixels, as shown in Figure 5. Compared to a single rectangular macropixel, two square macropixels increase the ratio of lower-scattering angle to higher-scattering angle deuterons detected by the spectrometer. This improves the spectrometer's performance, as will be discussed below. The ideal material and mass thickness of the deuteron absorber were not investigated, and simulations assumed no cross-talk between the two macropixels.

4.3 Size of the macropixels

Within the planar configuration, one can vary the size of the macropixels. Given an approximately collimated neutron source, an array of small macropixels is functionally equivalent to a single, larger macropixel, scaled up in all three dimensions, with the same converter foil area as the array.

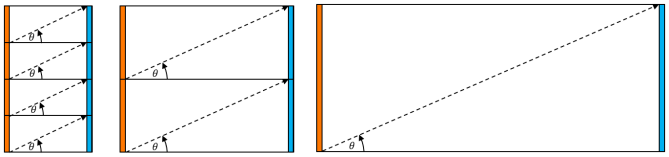

Figure 8: *Comparison of macropixel sizes. Macropixels of different sizes, if they are geometrically similar, have the same maximum angle. If they also have the same active area (in orange), they are functionally equivalent.*

As shown in Figure 8, an array of small macropixels and a single larger macropixel with the same area are equivalent in all relevant properties. The surface areas of the converter foils are the same, so the same number of neutrons will hit the converter foil, and the same number of deuterons will be produced, with the same energy and angle distributions. The small and large macropixels are geometrically similar to each other (in the technical sense), so the proportion of deuterons at each angle that reach the detector surface from the foil will be the same for both macropixel sizes. Thus, the energy and angle distribution of deuterons hitting the detector will be the same for an array of small macropixels as for a single, larger macropixel. The size of the CMOS pixels, which detect the individual deuterons, is independent of macropixel size, so macropixel size does not affect the spectrometer's ability to measure individual deuterons.

An array of small macropixels requires deuteron absorbers as walls between macropixels, to prevent cross-talk. These walls could introduce error. Some deuterons might penetrate the walls and enter other macropixels, or collide with the walls and lose energy, but still reach the detector. Additionally, neutrons that pass through the converter foil might interact with the walls and produce deuterons. An ideal wall material could minimize these concerns, but this was not investigated. Future work should determine the optimal material and thickness for the dividing walls.

The design with only two large macropixels was chosen for multiple reasons. The larger-macropixel design is simpler, because of its single dividing wall. Building a detector with many dividing walls would be more difficult and expensive. Secondly, in order to effectively absorb deuterons, the wall must have a non-trivial thickness. The wall must therefore occupy some of the geometrical cross-section of the spectrometer, reducing its active area and space-efficiency. Therefore, the fewer dividing walls, the greater the space-efficiency of the spectrometer.

5 Further considerations for optimization

In order for the spectrometer to have a high resolution, it must be able to determine the incident neutron spectrum. For this, two preconditions are necessary. First, the spectrometer must detect a large number of neutrons, so there are many points from which to determine the neutron spectrum. In optimizing the configuration of the detector surface and the material of the converter foil, maximizing the detection rate was the main concern. Second, the energy of each deuteron detected by the spectrometer must be predictive of the energy of the neutron producing the deuteron. Otherwise, the spectrometer would be unable to accurately measure the neutron spectrum. The ability to determine the energy of a neutron from the recoiled deuteron it produces will henceforth be called predictivity. The maximum scattering angle observed by the spectrometer and the mass thickness of the converter foil both present tradeoffs between the detection rate and the predictivity of the spectrometer.

5.1 Maximum observed scattering angle

The reaction producing the deuteron is an elastic collision between the incident neutron and the deuterium nucleus. Based on conservation of energy and momentum, the higher the scattering angle, the less energy the deuteron has, relative to the initial energy of the neutron. This is illustrated in Figure 9.

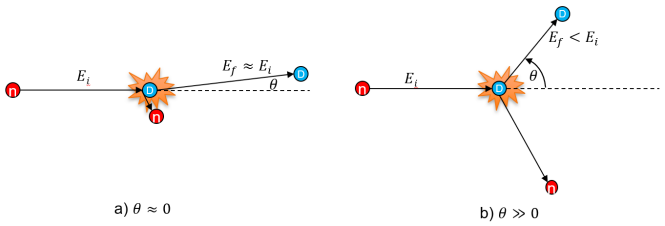

Figure 9: *Effects of scattering angle on deuteron energy. a) Low scattering angle. Deuterons at low scattering angles have energy close to that of the incident neutron. Because the deuteron has twice the mass of the neutron, the maximum energy transfer from the neutron to the deuteron is* $\frac{8}{9}E_i$*. b) High scattering angle. Deuterons at high scattering angles have substantially less energy than the incident neutron.*

For a spectrometer with perfect angular resolution, where the direction of each deuteron is known, this does not reduce predictivity, because the energy of the deuteron relative to the energy of the neutron is deterministically and exclusively based on the scattering angle. However, in a planar arrangement, where the detector surface is equal in size and shape to the converter foil, it is impossible to achieve high angular resolution, because any deuteron could have been produced anywhere on the converter foil. One potential solution would be making the detector surface much larger than the converter foil, but this would substantially reduce the space efficiency of the spectrometer. Therefore, only spectrometers without angular resolution were investigated.

The maximum scattering angle presents a tradeoff. Restricting the spectrometer to a low maximum scattering angle reduces the effects of energy loss from high scattering angle, which increases the predictivity; however, a low maximum scattering angle leads to a low detection rate. Conversely, a high maximum scattering angle leads to lower predictivity, but it allows a higher detection rate.

5.2 Mass thickness of the converter foil

The mass thickness of the converter foil also presents a tradeoff between the detection rate and predictivity of the spectrometer. In order to be detected, a neutron must collide with a deuterium atom in the converter foil. The greater the mass thickness of the converter foil, the more neutron-deuterium collisions, and the higher the detection rate.

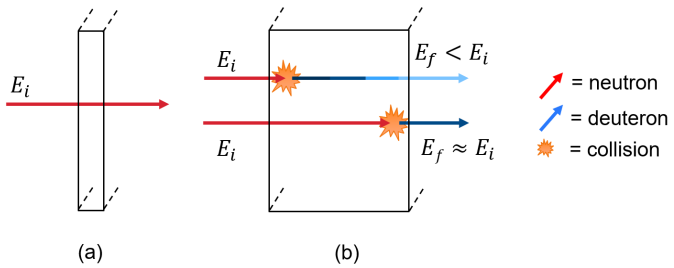

Figure 10: *Mass thickness considerations. a) Low mass thickness. If the mass thickness is too low, too many neutrons will pass through the foil without interacting. b) High mass thickness. If the mass thickness is too great, deuterons that are generated near the front of the foil will lose more energy in the foil than deuterons generated near the back of the foil, reducing the accuracy of energy measurements.*

Deuterons are charged particles, so as they travel through the converter foil, they lose energy.[8] Therefore, the greater the mass thickness through which a deuteron must travel, the more energy it loses. When a high-energy neutron produces a high-energy deuteron near the front of the converter foil, the deuteron loses energy before exiting the converter foil, and it is indistinguishable from a lower-energy deuteron produced by a lower-energy neutron towards the back of the converter foil. Thus, increasing the mass thickness decreases the predictivity of the the spectrometer. This tradeoff is illustrated in Figure 10. At large enough mass thicknesses, the energy loss is so great that the deuterons could fail to escape the foil, or range out. However, the foils investigated in this work were thin enough that the effects of deuterons ranging out were negligible, except at very high scattering angles.

5.3 Combinations of mass thickness and scattering angle

Mass thickness and scattering angle were tested in combination with each other because they are dependent on each other: the mass thickness affects the deuteron spectrum at each scattering angle. Simulations were run in MCNP to test combinations of mass thickness and scattering angle.

Each trial simulated a monoenergetic, collimated source, with an energy of 2.45 MeV and a total of 3×10^7 neutrons. The direction and energy of each deuteron produced were recorded as it left the converter foil. For each combination of mass thickness and maximum scattering angle, detection rate was calculated as the number of deuterons with scattering angles less than the maximum, divided by the number of incident neutrons. The predictivity was defined as the standard deviation divided by the mean for the energy spectrum of deuterons with scattering angles less than the maximum.

Simulations were performed for combinations of 15 maximum scattering angles, ranging from 2.5° to 90°, and 21 mass thicknesses, ranging from 15 $\mu g/cm^2$ to 4.8 mg/cm^2. The results are shown in Figure 11.

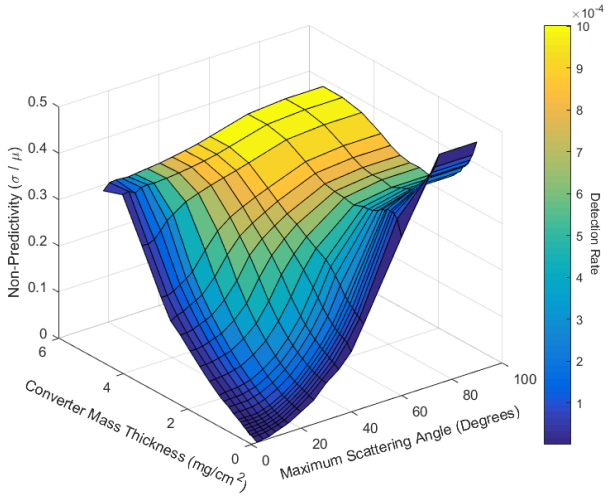

Figure 11: *Dependence of detection rate and predictivity on mass thickness and maximum scattering angle.*

These simulations matched the predicted effects of mass thickness and maximum scattering angle. Higher maximum scattering angles and higher mass thicknesses led to higher detection rates, but also to lesser predictivity. A plot of achievable combinations of predictivity and detection rates (Figure 12) shows an approximately linear bound separating achievable and unachievable combinations of predictivity and detection rate.

The geometry of these simulations differed from the geometry of an actual spectrometer with respect to the counting of deuterons at scattering angles close to the maximum. In the planar arrangement (Figure 6(a)), the converter foil and detector surface are placed at the two bases of a prism. The maximum scattering angle would be observed if a particle scatters from one corner of the converter foil to the opposite corner of the detector surface.

Most deuterons scattered at very small angles hit the detector surface, but few deuterons scattered close to the maximum scattering angle hit the detector surface, unless they are generated at the corner of the converter foil and scatter in exactly the right direction. Thus, even below the maximum scattering angle, deuterons at higher scattering angles are less likely to be detected than deuterons at lower scattering angles.

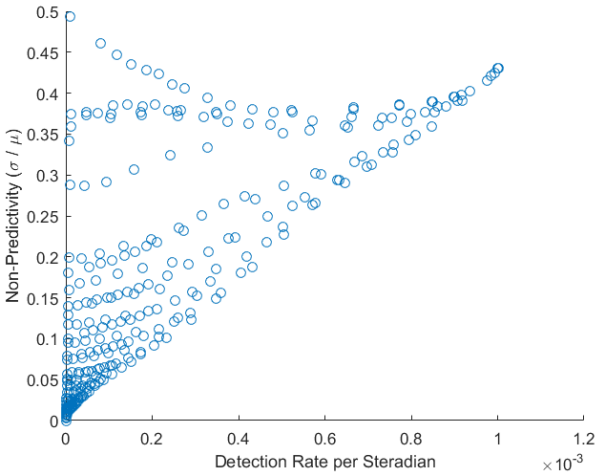

Figure 12: *Achievable predictivity-detection rate combinations, from the simulations shown in Figure 11. The ideal spectrometer would have low non-predictivity and high detection rate and would appear at the bottom right of the graph.*

Simulations indicated that for a square panel, the probability of detecting a deuteron decreases approximately linearly, from 100% detection at a scattering angle of 0° to approximately 0% detection at the maximum scattering angle.

The equal weighting of deuterons at all angles less than the maximum scattering angle artificially increases the detection rate and decreases the predictivity of each trial. However, it does not change the relative detection rate and predictivity of each trial, which were the purpose of this set of simulations. All subsequent simulations accounted for this issue.

6 Modeling the deuteron spectrum

As shown in Eq. 3, the relationship between the T_i, σ, and $\langle E_n \rangle$ of the neutron spectrum follows $T_i \propto \sigma^2/\langle E_n \rangle$. The σ is squared and varies more than $\langle E_n \rangle$, so apparent temperature can be approximated using only σ. Therefore, the analysis of simulated data focused on determining the σ of the neutron spectrum.

The deuteron spectrum is equal to the convolution of the neutron spectrum with the energy spectrum of deuterons scattered by a deuterated plastic foil, taking into account the scattering angles observed. Based on kinematics, the energies of scattered deuterons at each angle should be proportional to the energy of the incident neutron. Thus, the spectra produced by neutrons of different energies should be geometrically similar to each other, but scaled along the energy axis. For small enough differences in neutron energy, this transformation can be approximated by a translation along the energy axis. In theoretical modeling, therefore, the same spectrum of scattered deuteron energies, with respect to the neutron energy, was used for all neutron energies.

As shown in Figure 13, there is a strong correlation between energy and scattering angle. Additionally,

the scattering spectrum of deuterium with respect to energy is approximately linear at high energies. At energies of below 1.5 MeV, the probability density is approximately constant. However, because the proportion of high-angle deuterons that hit the detector surface approaches zero near the maximum scattering angle, the spectrum observed by the spectrometer contains fewer high-angle, low-energy deuterons than the spectrum shown in Figure 13. As a result, the overall scattering spectrum of deuterium with respect to energy, accounting for the effects of the scattering angles observed, can be approximated as a right triangle, with one leg on the x-axis, one vertical leg, and the peak on the right.

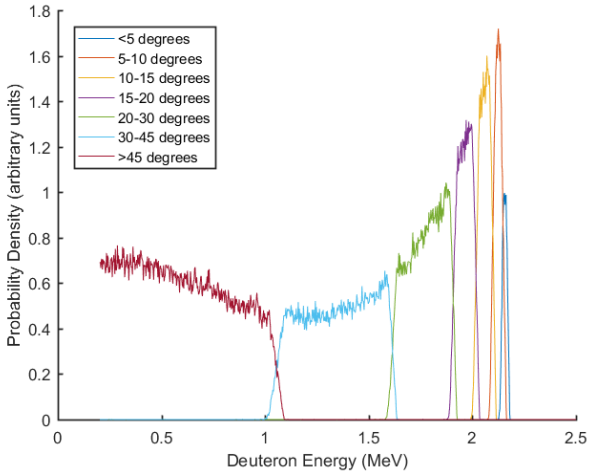

Figure 13: *Spectrum of scattered deuterons with respect to energy, as produced by 2.45 MeV neutrons incident on a very thin foil of deuterated plastic* ($\langle \rho l \rangle = 0.1\ \mu g/cm^2$). *The slight energy overlap between different angle bins is due to energy loss of deuterons within the foil. The under-5° bin has the fewest deuterons because it subtends the smallest solid angle. The simulation did not track deuterons with energies below* 0.2 MeV, *because they were unlikely to escape the foil and hit the detector.*

Convolutions of such a right triangle with Gaussian distributions of different widths (Figure 14) approximate the dependence of the observed deuteron spectrum on the width of the incident neutron spectrum. When the neutron spectrum is narrow compared to the triangle, the resultant deuteron spectrum is roughly triangular, with a long tail at low energies and very few particles more energetic than the peak of the distribution. When the neutron spectrum is wide compared to the triangle, the resultant deuteron distribution becomes more Gaussian in shape.

All of the theoretical deuteron distributions in Figure 14 have low-energy tails of similar width. However, the width of the high-energy tail of the deuteron distribution is highly sensitive to the width of the neutron distribution. Therefore, the spectrometer uses the deuteron spectrum's width to the right of its peak (WROP) to predict the width of the neutron distribution. Note that the *peak* of the observed deuteron distribution refers to the energy at which the probability distribution for detected deuteron energy is at a maximum, not the maximum observed deuteron energy. Even though all deuterons to the right of the peak have low scattering angles, arrangements with high maximum scattering angles were still considered, because deuterons

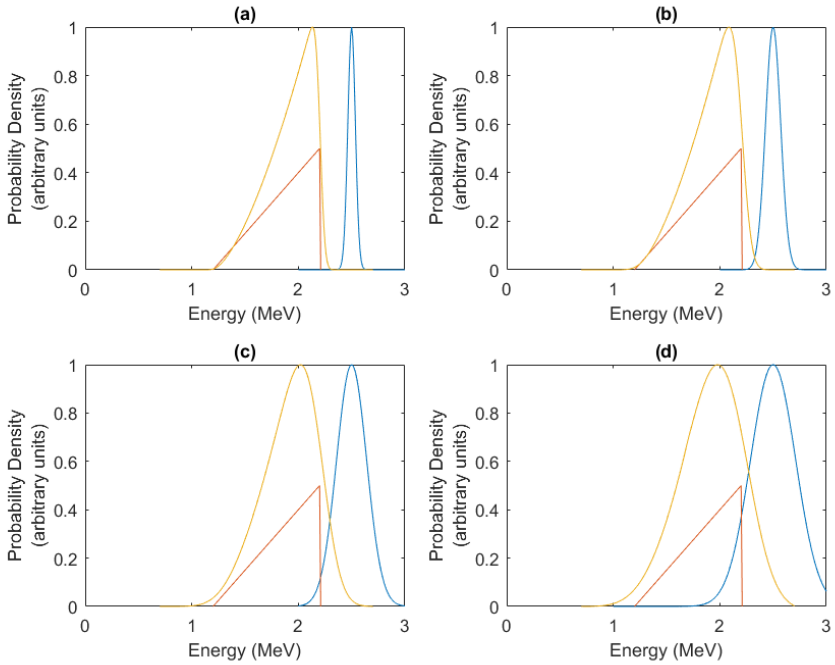

Figure 14: *Approximations of deuteron spectra (yellow) as convolutions of Gaussian neutron spectra of different widths (blue) with a right triangle (red) that roughly approximates the overall scattering spectrum of deuterium produced by 2.45 MeV neutrons. Subfigures a, b, c, and d show progressively wider neutron distributions.*

with higher scattering angles can increase the resolution for determining the peak of the distribution.

Calculating the WROP requires determining the peak of the deuteron distribution and the maximum energy. The maximum energy was defined as a high percentile of the distribution. After tests of multiple percentiles, the 99.5^{th} percentile was found to be the most reliable.

In trials with low neutron yields or thin foils, the number of deuterons detected was relatively low. As a result, the deuteron spectrum was noisy, so the mode of the measured distribution was not always an accurate representation of its peak. Therefore, the peak was calculated by finding the smallest energy intervals that contained 2, 4, 6, 8, and 10% of the observed deuterons. These intervals were assumed to be centered on the peak, so the midpoints of the five intervals were averaged together to determine the peak of the distribution. This method prevented noisiness in the spectrum from affecting the determination of the peak. The deuteron spectrum from 1 keV fusion in Figure 15 below provides an example. The spectrum had two local maxima, separated by a slight dip, and the algorithm determined the peak to be between the two local maxima.

7 Final optimization of the spectrometer design

To determine the optimal mass thickness and maximum scattering angle, simulations were done for combinations of 20 mass thicknesses, ranging from 1.0×10^{-5} to 2.0×10^{-2} g/cm^2, and 17 maximum scattering angles, in 5° increments from 5° to 85°. Each combination was evaluated for its performance over three temperature intervals: $0.1-1.0$ keV, $0.1-10$ keV, and $1.0-10$ keV. The simulations exhibited the predicted relation between the WROPs of the neutron and deuteron spectra. Figure 15 shows examples of the determination of the WROPs of deuteron and neutron spectra, and Figure 16 shows examples of the correlation between neutron WROP and deuteron WROP.

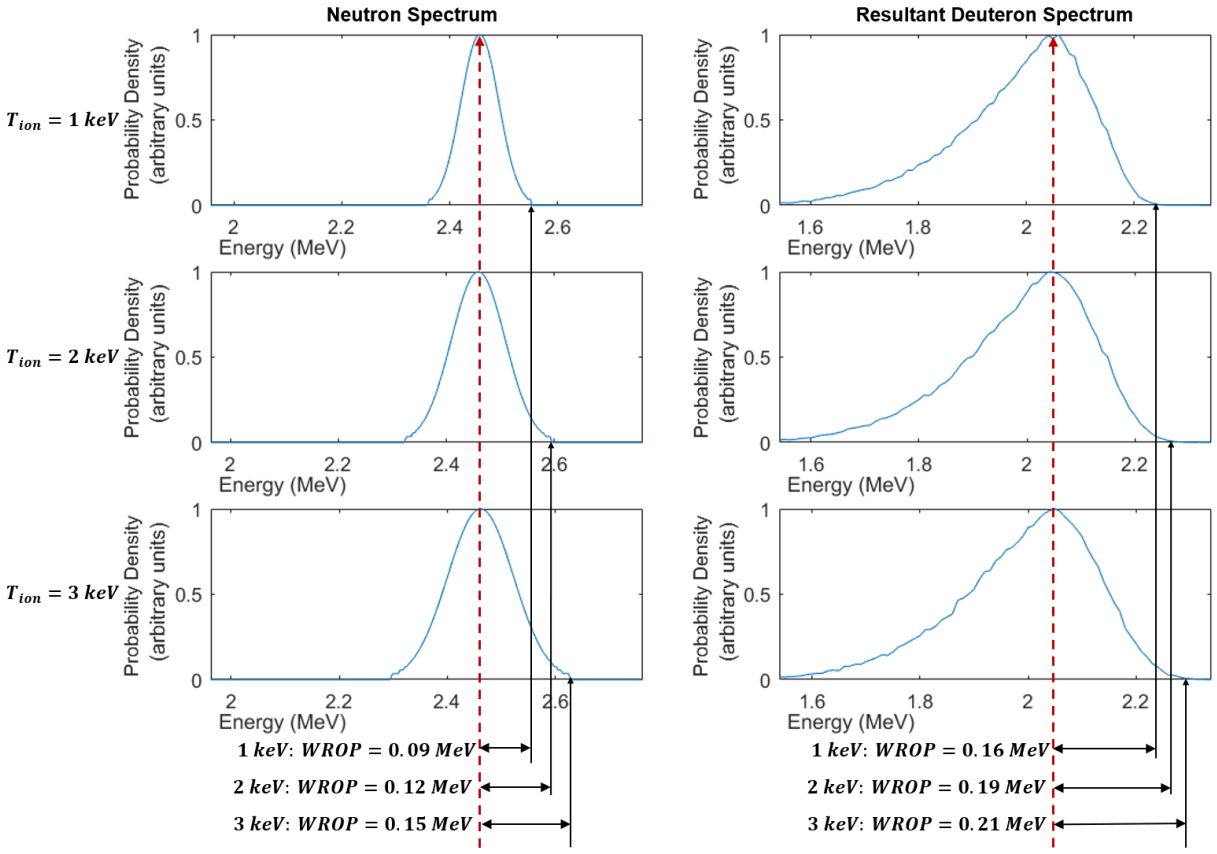

Figure 15: *Example of the use of WROP to differentiate between neutron spectra of different widths. The range of the energy axis is different between the neutron and deuteron spectra, but the scale is consistent. For all three examples, the mass thickness, maximum scattering angle, and neutron count were* 600 $\mu g/cm^2$, 35°, *and* 10^{10}, *respectively. These were among the least noisy deuteron spectra measured, due to the high neutron count and mass thickness.*

The performance of the spectrometer was evaluated for detection rate and sensitivity. The calculation of WROP focuses on the deuterons to the right of the peak, so the detection rate only considered deuterons to the right of the peak. The sensitivity is a measure of the ability of the spectrometer to discriminate

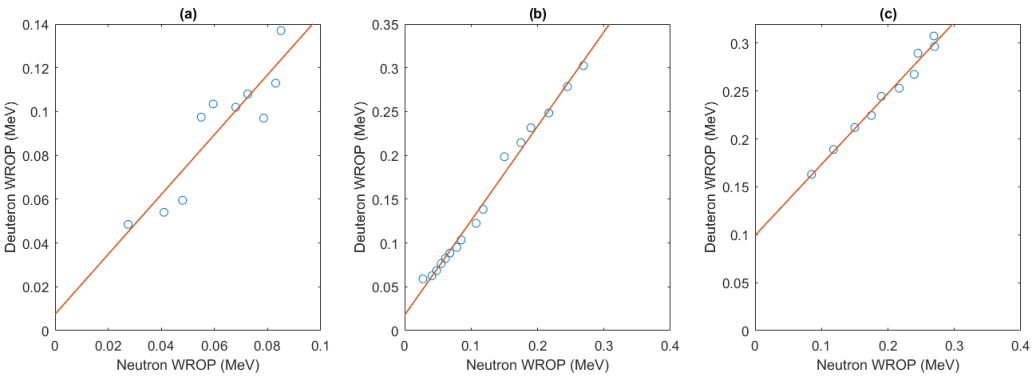

Figure 16: *Three examples of neutron and deuteron WROPs, with varying degrees of correlation. The regression lines from these three data sets had slopes of 1.37, 1.08, and 0.74 and R^2 values of 0.827, 0.991, and 0.983, respectively. The simulations used the optimized mass thicknesses and maximum scattering angles listed in Table 2 below. a) Neutron and deuteron WROPs from 10^8 neutrons at temperatures of 0.1-1.0 keV. b) Neutron and deuteron WROPs from 10^9 neutrons at temperatures of 0.1-10 keV. c) Neutron and deuteron WROPs from 10^{10} neutrons at temperatures of 1.0-10 keV. Subfigure c includes the examples shown in Figure 15.*

between different ion temperatures. The sensitivity was calculated based upon a regression between the deuteron WROP and the incident neutron WROP, as illustrated in Figure 16. To have a high sensitivity, the deuteron WROP must be highly correlated with the neutron WROP, and the deuteron WROP should respond as much as possible to changes in the neutron WROP. Therefore, the sensitivity was defined as the product of the slope of the regression line between neutron WROP and deuteron WROP $\left(\frac{d(WROP_{deuteron})}{d(WROP_{neutron})}\right)$ and the square of the R^2 value of the linear regression between neutron WROP and deuteron WROP.

The spectrometer design was optimized for each temperature range by choosing the mass thickness-maximum scattering angle combination that produced the highest detection rate while maintaining a high sensitivity. The detection rate value for each trial was reliable, but the sensitivity showed more fluctuation. The detection rate to the right of the peak ranged from 10^{-7} to 10^{-5} deuterons per incident neutron. The deuteron WROP was therefore based on a small quantity of deuterons, relative to the incident neutron count. This causes uncertainty in the determination of the deuteron WROP, which causes uncertainties in sensitivity. An anomolous deuteron WROP value could substantially change the $\frac{d(WROP_{deuteron})}{d(WROP_{neutron})}$, which would affect the measured sensitivity.

A comparison of the results from many trials of the same conditions would yield a more accurate measure of the sensitivity. However, performing many trials of each run was prohibitively computation-intensive. Instead, the reliability of the sensitivity measurement was determined by comparing each trial to the trials of the same mass thickness and slightly different scattering angles. Under the assumption that a small change in maximum scattering angle should produce only small changes in sensitivity, a trial's sensitivity was considered to be more reliable if it was similar to the sensitivity from trials with the same

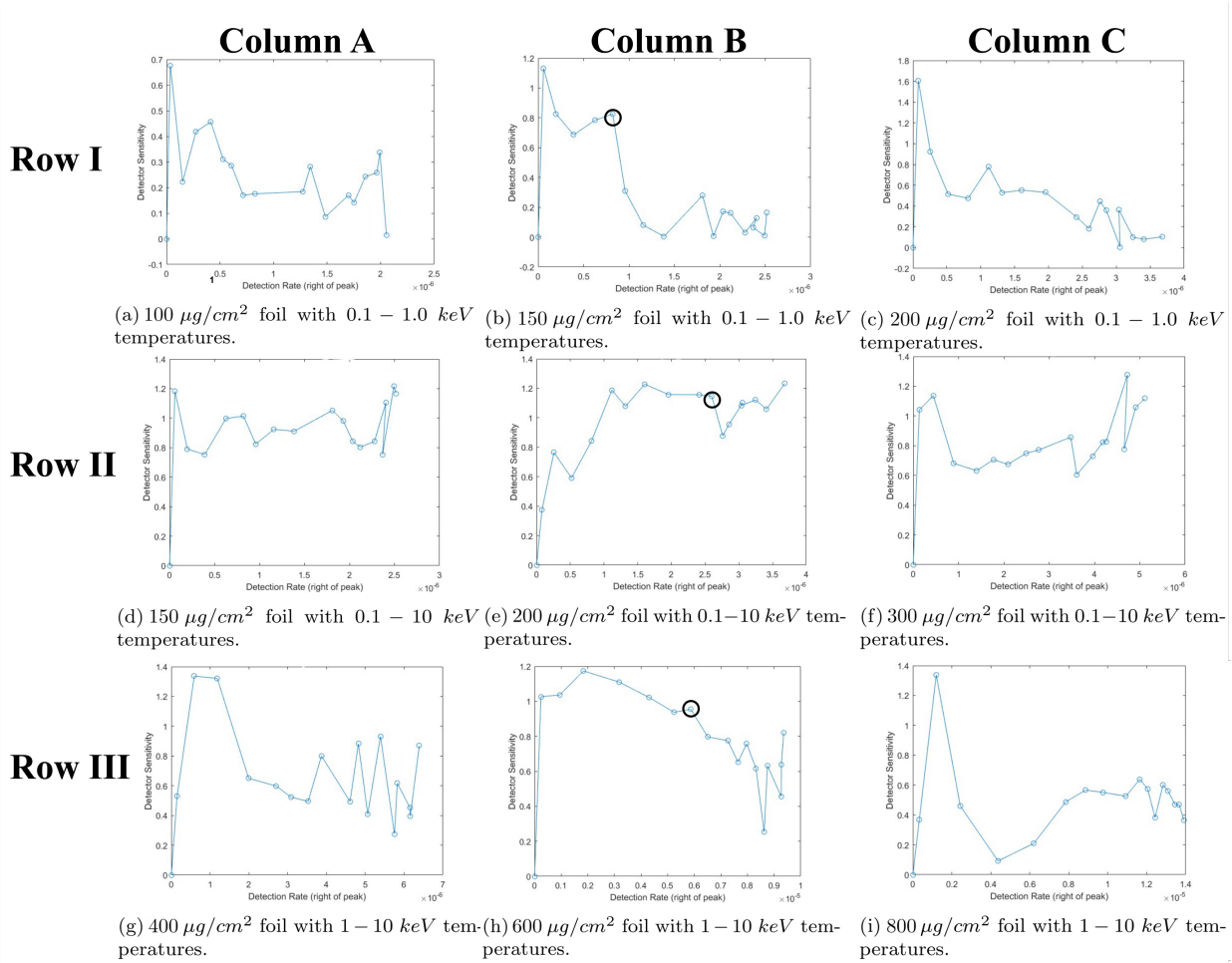

(a) 100 $\mu g/cm^2$ foil with $0.1 - 1.0$ keV temperatures.

(b) 150 $\mu g/cm^2$ foil with $0.1 - 1.0$ keV temperatures.

(c) 200 $\mu g/cm^2$ foil with $0.1 - 1.0$ keV temperatures.

(d) 150 $\mu g/cm^2$ foil with $0.1 - 10$ keV temperatures.

(e) 200 $\mu g/cm^2$ foil with $0.1-10$ keV temperatures.

(f) 300 $\mu g/cm^2$ foil with $0.1-10$ keV temperatures.

(g) 400 $\mu g/cm^2$ foil with $1-10$ keV temperatures.

(h) 600 $\mu g/cm^2$ foil with $1-10$ keV temperatures.

(i) 800 $\mu g/cm^2$ foil with $1 - 10$ keV temperatures.

Figure 17: *Detection rate and sensitivity for a range of maximum scattering angles, mass thicknesses, and temperatures. For each row, Column A shows a foil that is too thin, Column B shows the chosen foil, and Column C shows a foil that is too thick. Each graph shows data points at maximum scattering angles from* $0°$ *to* $85°$*, in* $5°$ *increments, beginning at the origin. In Column B, the circled data point represents the chosen maximum scattering angle. Row I (a-c): Optimization for 0.1-1.0 keV. Row II (d-f): Optimization for 0.1-10 keV. Row III (g-i): Optimization for 1.0-10 keV.*

mass thickness and similar maximum scattering angles.

For each temperature range investigated, the detection rate and sensitivity are shown in Figure 17 for a range of maximum scattering angles, at mass thicknesses just less than, equal to, and just greater than the chosen mass thickness. The chosen mass thickness-maximum scattering angle combinations are listed in Table 2.

Table 2: *Optimized Design Parameters*

Ion temperature range (keV)	Optimized mass thickness ($\mu g/cm^2$)	Optmizied maximum scattering angle ($°$)
0.1-1.0	150	25
0.1-10	200	50
1.0-10	600	35

8 Performance of the chosen spectrometer designs

Detailed simulations were carried out to evaluate the performance of these three spectrometer designs. Each spectrometer was simulated over 10-16 temperatures in the range for which the spectrometer was optimized, at incident neutron counts of 10^7, 10^8, 10^9, and 10^{10}.

For each design at each yield, a linear regression between the WROP of the incident neutron spectrum and the WROP of the deuteron spectrum was calculated, based on simulations at different temperatures. This regression was then used to calculate a predicted neutron WROP based on each deuteron WROP. To measure the accuracy of the spectrometer design, the mean percent error between the actual neutron WROP and the predicted neutron WROP was used. The results are shown in Figure 18.

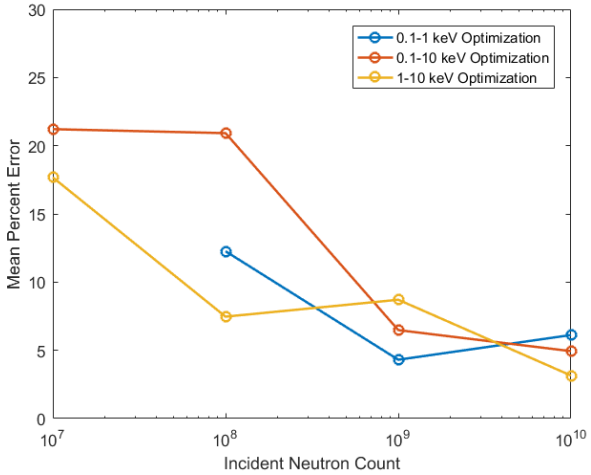

Figure 18: *The mean percent error for WROP prediction at different yields. Each mean percent error is based upon simulations at 10-16 temperatures within the temperature range for which the design was optimized. There was no meaningful ability to predict the WROP for 0.1-1.0 keV optimization at a yield of* 10^7*, so the mean percent error is not shown at that point.*

The mean percent error was under 25% for all cases studied, with the exception of 10^7 neutrons at ion temperatures of $0.1 - 1.0\ keV$. In that range, so few deuterons were detected that no useful measurements could be made. The trends in these results match theoretical predictions. The spectrometer designed for $1.0 - 10\ keV$ generally has lower error than the spectrometer designed for $0.1 - 1.0\ keV$, due to the greater WROPs at higher temperatures. Additionally, the error tends to decrease as the yield increases, because the greater number of deuterons detected reduces the uncertainty of the measurements.

The deuteron data was also used to estimate the ion temperature, using Eq. 3. The neutron spectrum is a normal distribution,[3] meaning that its 99.5^{th} percentile is 2.576 standard deviations above the mean. Therefore, a neutron distribution with a WROP of W has a standard deviation of $\sigma = W/2.576$, yielding a temperature equation of

$$T_i = \frac{W^2\,(m_n + m_\alpha)}{2\,(2.576^2)\,m_n \langle E_n \rangle}. \tag{5}$$

The determination of $\langle E_n \rangle$ was not investigated. The peak of the deuteron distribution was used, but this introduced substantial error, because the deuteron energy peak is significantly lower than the neutron energy peak *(see Figure 15)*. Therefore, a second linear regression was run on the calculated T_i values in order to account for the difference in neutron and deuteron peaks. This formula was used to generate a calculated ion temperature for each trial, and the mean percent error was calculated for each spectrometer design and yield. The results are shown in Figure 19.

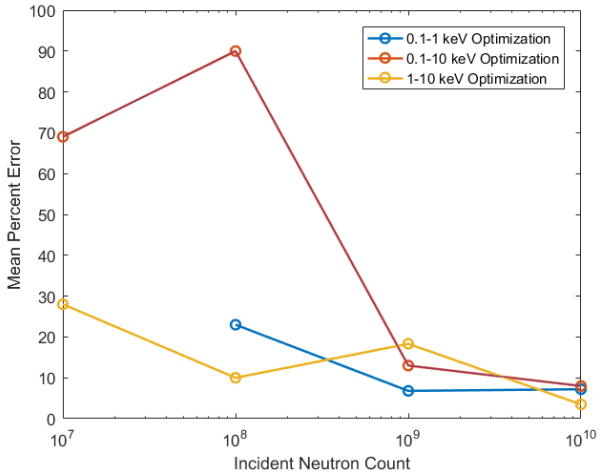

Figure 19: *The mean percent error for ion temperature prediction at different yields. There was no meaningful ability to predict the ion temperature for 0.1-1.0 keV optimization at a yield of* 10^7*, so the mean percent error is not shown. Developing a more accurate method of determining* $\langle E_n \rangle$ *would likely improve the temperature measurements.*

The trends for temperature prediction are similar to the trends for WROP prediction: higher temperatures and higher yields tend to reduce error. The error in temperature prediction is generally greater than the error in WROP prediction. One reason for this is that temperature is proportional to WROP squared, as shown in Eq. 5, so errors in WROP prediction are magnified. The lack of a reliable method of calculating $\langle E_n \rangle$ from the deuteron spectrum causes additional error. It is likely that the $\langle E_n \rangle$ can be deduced from the deuteron spectrum, and further work should explore this possibility.

The neutron yield at FuZE is on the order of 10^5 neutrons per pulse, over 4π steradians.[2] It follows that any spectrometer would observe many fewer than 10^5 neutrons per pulse. Given that the spectrometer described here must observe at least 10^7 neutrons to make useful measurements, it is not efficient enough to be used at FuZE. However, other existing fusion reactors have much higher yields. For example, JET has achieved neutron yields of over 10^{15} neutrons,[10] with ion temperatures of a few keV.[11] At such yields, the spectrometer could function even if the proportion of neutrons that hit the spectrometer is 10^{-5} or less. This would require a few tens of Icarus chips, which could be feasible.

9 Areas for further investigation

9.1 Measurement of the deuteron energy spectrum

This work did not investigate the process of determining the deuteron spectrum from the signal from the CMOS detector. The extraction of the deuteron spectrum could be a significant source of error, for multiple reasons.

The total energy deposited by a deuteron is the integral of $\frac{dE}{dx}$ over its path, or

$$\Delta E = \int_x dE = \int_x \left(\frac{dE}{dx}\right) dx. \tag{6}$$

Therefore, the longer the path length, the greater the energy deposition. The path length of a deuteron with angle ϕ from the normal is inversely proportional to $\cos\phi$. The chosen spectrometer arrangements have maximum scattering angles of 25°, 35°, and 50°, which permit variations in path length of up to 10%, 22%. and 55%, respectively. This effect could be modeled. However, compensating for the uncertainty introduced by angle variations could require a larger data sample, which requires a higher detection rate.

If multiple deuterons hit the same pixel of Icarus within 1.5 ns, the pixel does not have time to reset, and it records the two events identically to a single, higher-deposition event. Such double hits compromise the accuracy of the detector. Statistical analysis can be used to determine the maximum deuteron flux, and therefore the maximum neutron flux, that the detector can observe without substantial error from double hits. Given the low efficiency of the detector, the maximum flux is unlikely to be a limiting factor.

The CMOS detector is primarily designed to detect charged particles, such as protons and deuterons. However, it is possible for neutrons to interact with the CMOS detector as well. Considering that the optimal detector arrangements have efficiencies of less than 1.0×10^{-5}, the neutron flux on the detector surface will be much greater than the deuteron flux. If the neutrons interact with the CMOS detector at a non-negligible rate, it could produce background noise that limits the ability to observe the deuteron signal.

9.2 Accounting for shifts of the neutron and deuteron peaks

As previously discussed, a method of determining the $\langle E_n \rangle$ would substantially improve temperature prediction. Because the neutron spectrum is Gaussian, the mean energy is equivalent to the peak of the spectrum. Thus, $\langle E_n \rangle$ could be calculated by determining the relation between the peak of the deuteron spectrum and the peak of the neutron spectrum. Two factors complicate the determination of this relation.

Firstly, the peak of the neutron spectrum shifts depending on the temperature.[3] Secondly, as shown in Figure 14, the location of the peak of the deuteron spectrum with respect to the peak of the neutron spectrum changes based on the width of the neutron spectrum. Therefore, the relationship between the peaks is more

complex than the model used in this work, and future work should develop more accurate models for this relationship.

9.3 Discrimination between beam-target and thermonuclear fusion

Another use of neutron spectrometry is the discrimination between beam-target fusion, where all fusion reactions involve accelerated particles, and thermonuclear fusion, where the thermal energy is enough to cause fusion. Discrimination between the two requires the measurement of the location of the peak of the neutron distribution, separately from the measurement of the width of the neutron distribution. The ability to extract this value from the deuteron signal was not investigated.

10 Conclusion

A neutron spectrometer was designed for use with 2.45 MeV neutrons from D-D fusion. The spectrometer consists of a neutron-to-deuteron converter foil and an Icarus hCMOS chip, which measures the deuteron spectrum. Deuterated plastic was selected as the material of the converter foil, and the converter foil was placed parallel to the detector surface. Three optimal combinations of the mass thickness of the converter foil and the maximum observable deuteron scattering angle were developed, depending on the apparent ion temperature range of the fusing plasma.

A model was developed to determine the apparent ion temperature of the fusing plasma, by correlating the widths of the observed deuteron spectrum and the incident neutron spectrum. At incident neutron counts of 10^9 and above, apparent ion temperature prediction was accomplished with mean error of less than 20% across all temperature ranges studied.

The spectrometer is time-independent, enabling its use with reactors with durations beyond the limits of time-of-flight spectrometers. The accuracy of the spectrometer is highly dependent upon the incident neutron count, and although it is unusable at very low-yield reactors, such as FuZE, the design has the potential to be applied at higher-yield reactors. A prototype of the spectrometer will be built and tested at LLE, as a proof of concept.

11 Acknowledgements

This work would not have been possible without the help of many people. Most of all, I would like to thank my advisor, Dr. Chad Forrest. From framing this project to guiding me with the research process to providing feedback on this report, his help has been invaluable. I am also indebted to William Scullin, for handling all the technological challenges that arose during this project. Without his assistance setting

up and trouble-shooting the computer environment, I would never have been able to run all the simulations that formed the basis of this research.

I would also like to thank Jonathan Davies, for explaining the intended use of the spectrometer at FuZE; Steve Ivancic, for providing the specifications of the Icarus chip; and Vladimir Glebov, for giving me valuable feedback on my presentation. Lastly, I am grateful to Dr. Stephen Craxton, for managing the Summer Research Program. His supervision ensured that everything ran smoothly, and his guidance was essential to the oral and written presentation of my work.

References

[1] G. M. McCracken and P. E. Stott, *Fusion: the energy of the universe*. Burlington, MA: Elsevier Academic Press, 2005.

[2] Y. Zhang, U. Shumlak, B. A. Nelson, R. P. Golingo, T. R. Weber, A. D. Stepanov, E. L. Claveau, E. G. Forbes, Z. T. Draper, J. M. Mitrani, H. S. McLean, K. K. Tummel, D. P. Higginson, and C. M. Cooper, "Sustained neutron production from a sheared-flow stabilized Z pinch," *Physical Review Letters*, vol. 122, no. 13, p. 135001, 2019.

[3] H. Brysk, "Fusion neutron energies and spectra," *Plasma Physics*, vol. 15, no. 7, pp. 611–617, 1973.

[4] D. Thomas, "Neutron spectrometry," *Radiation Measurements*, vol. 45, no. 10, pp. 1178 – 1185, 2010.

[5] J. A. Frenje, D. T. Casey, C. K. Li, F. H. Séguin, R. D. Petrasso, V. Y. Glebov, P. B. Radha, T. C. Sangster, D. D. Meyerhofer, S. P. Hatchett, S. W. Haan, C. J. Cerjan, O. L. Landen, K. A. Fletcher, and R. J. Leeper, "Probing high areal-density cryogenic deuterium-tritium implosions using downscattered neutron spectra measured by the magnetic recoil spectrometer," *Physics of Plasmas*, vol. 17, no. 5, p. 056311, 2010.

[6] C. J. Forrest, V. Y. Glebov, V. N. Goncharov, J. P. Knauer, P. B. Radha, S. P. Regan, M. H. Romanofsky, T. C. Sangster, M. J. Shoup, and C. Stoeckl, "High-dynamic-range neutron time-of-flight detector used to infer the D(t,n)4He and D(d,n)3He reaction yield and ion temperature on OMEGA," *Review of Scientific Instruments*, vol. 87, no. 11, p. 11D814, 2016.

[7] L. D. Claus, "An overview of the Sandia Labs ultra-fast x-ray imager (UXI) program," 2015.

[8] W. R. Leo, *Techniques for nuclear and particle physics experiments: a how-to approach*. New York: Springer-Verlag, 1987.

[9] X-5 Monte Carlo Team, MCNP —A General Monte Carlo N-particle transport code, Version 5, Los Alamos National Laboratory, Los Alamos, NM, Report LA-UR-03-1987 (2008).

[10] P. van Belle, O. N. Jarvis, G. Sadler, S. de Leeuw, P. D'Hondt, and M. Pillon, "Calibration of the JET neutron yield monitors using the delayed neutron counting technique," *Review of Scientific Instruments*, vol. 61, no. 10, pp. 3178–3180, 1990.

[11] P. H. Rebut, R. J. Bickerton, and B. E. Keen, "The Joint European Torus: installation, first results and prospects," *Nuclear Fusion*, vol. 25, no. 9, pp. 1011–1022, 1985.